Solar Phys (2009) 256: 269–284
DOI 10.1007/s11207-009-9339-4

Solar – Terrestrial Simulation in the STEREO Era: The 24 – 25 January 2007 Eruptions

N. Lugaz · A. Vourlidas · I.I. Roussev · H. Morgan

Received: 26 November 2008 / Accepted: 23 March 2009 / Published online: 7 April 2009

Abstract The SECCHI instruments aboard the recently launched STEREO spacecraft enable for the first time the continuous tracking of coronal mass ejections (CMEs) from the Sun to 1 AU. We analyze line-of-sight observations of the 24 – 25 January 2007 CMEs and fill the 20-hour gap in SECCHI coverage in 25 January by performing a numerical simulation using a three-dimensional magneto-hydrodynamic (MHD) code, the Space Weather Modeling Framework (SWMF). We show how the observations reflect the interaction of the two successive CMEs with each other and with the structured solar wind. We make a detailed comparison between the observations and synthetic images from our model, including time-elongation maps for several position angles. Having numerical simulations to disentangle observational from physical effects, we are able to study the three-dimensional nature of the ejections and their evolution in the inner heliosphere. This study reflects the start of a new era where, on one hand, models of CME propagation and interaction can be fully

STEREO Science Results at Solar Minimum
Guest Editors: Eric R. Christian, Michael L. Kaiser, Therese A. Kucera, O.C. St Cyr

Electronic supplementary material The online version of this article (http://dx.doi.org/10.1007/s11207-009-9339-4) contains supplementary material, which is available to authorized users.

N. Lugaz (✉) · I.I. Roussev · H. Morgan
Institute for Astronomy, University of Hawaii-Manoa, 2680 Woodlawn Dr., Honolulu, HI 96822, USA
e-mail: nlugaz@ifa.hawaii.edu

I.I. Roussev
e-mail: iroussev@ifa.hawaii.edu

H. Morgan
e-mail: hmorgan@ifa.hawaii.edu

A. Vourlidas
Code 7663, Naval Research Laboratory, Washington, DC 20375, USA
e-mail: vourlidas@nrl.navy.mil

H. Morgan
Sefydliad Mathemateg a Ffiseg, Prifysgol Aberystwyth, Ceredigion, SY23 3BZ, Cymru, UK

tested by using heliospheric observations and, on the other hand, observations can be better interpreted by using global numerical models.

Keywords Coronal mass ejections (CMEs) · MHD · Solar-terrestrial relation · Heliospheric observations

1. Introduction

Although Coronal Mass Ejections (CMEs) have been observed and studied extensively since the late 1960s (see reviews by Schwenn *et al.*, 2006, and Roussev and Sokolov, 2006), there had been no continuous dedicated remote-sensing observations of the heliosphere between 0.15 and 1 AU from the end of the *Helios* missions in the early 1980s to the launches of the *Solar Mass Ejection Imager* (SMEI) and the *Solar Terrestrial Relations Observatory* (STEREO) in 2003 and 2006, respectively. The in-depth study of the evolution of CMEs in the heliosphere had to rely solely on numerical models, mostly for "generic" fast CMEs (*e.g.*, see Odstrčil and Pizzo, 1999, and Manchester *et al.*, 2004). Only in the past two years have there been Sun-to-Earth numerical simulations of real events (*e.g.*, Chané *et al.*, 2006; Lugaz *et al.*, 2007; Tóth *et al.*, 2007). Particular attention has been given to the numerical modeling of CMEs at or near solar minimum, especially the 12 May 1997 CME (Odstrcil, Riley, and Zhao, 2004; Wu *et al.*, 2007; Cohen *et al.*, 2008a; Titov *et al.*, 2008). One reason for this focus is that the solar wind is believed to be simpler and steadier during solar minimum than during solar maximum. Therefore, solar minimum is thought to be the perfect time period to study the evolution of isolated CMEs. However, these previous works have not been totally successful in reproducing the observed transit time and the measured plasma parameters at 1 AU. Possible reasons for this failure are that the initial speed of the CME is not well constrained because Earth-directed CMEs appear as halo events and that there are no observations between $32 R_{\odot}$ and Earth. Therefore, studying limb CMEs with remote heliospheric observations should help better constrain the existing solar wind and eruption models.

The two events on 24 and 25 January 2007 were the first fast CMEs observed by the Sun Earth Connection Coronal and Heliospheric Investigation (SECCHI) suite (Howard *et al.*, 2008). Observations by the Heliospheric Imagers have been reported in Harrison *et al.* (2008) and numerical simulations have been performed by a number of groups and reported in publications (Lugaz *et al.*, 2008) and at meetings (*e.g.*, Webb *et al.*, 2008). In contrast to the event of 12 May 1997, this was not an isolated event but two successive CMEs, which are believed to have interacted on their way to 1 AU. Interacting CMEs are not uncommon, especially near solar maximum (Gopalswamy *et al.*, 2002) and there have been recent efforts to model them numerically (Odstrcil *et al.*, 2003; Lugaz, Manchester, and Gombosi, 2005b; Lugaz *et al.*, 2007; Xiong *et al.*, 2006). Even though CME – CME interactions are less frequent near solar minimum, there have been few reported cases, notably the 11 April 1997 geomagnetic storm, which is thought to have been caused by two CMEs (Berdichevsky *et al.*, 1998).

Studying the 24 – 25 January 2007 CMEs is important for future space weather predictions, because interacting CMEs are a major cause of large geomagnetic storms (Zhang *et al.*, 2007). It is also the first time that we can track this type of event in the heliosphere with actual observations. However, there are a few downsides. First of all, these were limb CMEs; therefore there were no *in situ* observations at Earth (nor by the STEREO spacecraft). Also, limb events (with respect to the observing spacecraft), such as these CMEs, may become

undetectable by SECCHI/Heliospheric Imagers as well as SMEI at large elongation angles (Vourlidas and Howard, 2006). In addition, the passage of Comet McNaught increased the background emission significantly in the southeastern quadrant of the observations at the time of the eruptions. Last, but most importantly, there was a 20-hour data gap in the SECCHI coverage, which coincided with the likely time of the interaction between the ejections.

Detailed studies of synthetic line-of-sight images have been performed by a number of groups in the past few years (Chen and Krall, 2003; Manchester *et al.*, 2004; Lugaz, Manchester, and Gombosi, 2005a; Odstrcil, Pizzo, and Arge, 2005; Riley *et al.*, 2008). Comparison of such synthetic observations with real observations by the Large Angle and Spectrometric Coronagraph experiment (LASCO), SMEI, or STEREO has only been done in the past three years for a few selected events during or close to solar maximum (Lugaz *et al.*, 2007; Manchester *et al.*, 2008; Sun *et al.*, 2008).

In this article, we report our efforts to understand the 24 – 25 January 2007 CMEs by means of three-dimensional (3-D) magnetohydrodynamic (MHD) simulations using the Space Weather Modeling Framework (SWMF) developed at the University of Michigan (Tóth *et al.*, 2005). In Section 2, we discuss the observations as well as the simulation setup. In Section 3, we discuss the evolution of the two CMEs in the heliosphere and their interactions, before comparing synthetic line-of-sight images with real ones, including time-elongation plots in Section 4. We conclude and discuss the main findings of our investigation and their consequences for future observations of CMEs by STEREO in Section 5.

2. The Solar Eruptions of 24 – 25 January 2007

2.1. LASCO and SECCHI Coronagraphs and Imagers

LASCO, onboard the *Solar and Heliospheric Observatory* (SOHO), has two working coronagraphs observing the solar corona from $2.1\,R_\odot$ to about $32\,R_\odot$ with a cadence of about 40 minutes (Brueckner *et al.*, 1995). The coronagraphs and heliospheric imagers part of the SECCHI investigation onboard STEREO are COR-1, COR-2, Heliospheric Imager 1, and Heliospheric Imager 2 (HI-1 and HI-2, respectively). Their fields of view are 2.13° ($4\,R_\odot$ with a $1.5\,R_\odot$ occulting disk), 8° ($15\,R_\odot$ with a $2\,R_\odot$ occulting disk), 20°, and 70°, respectively. Also, the HIs are not pointed at the Sun but along the Sun – Earth line and their fields of view are offset by an angle of 13.65° and 53.35° with respect to the Sun – spacecraft line, respectively (Howard *et al.*, 2008). At the time of the ejections, STEREO was in its commissioning phase and STEREO-A was rolled by 22.4° from the solar north, which resulted in HI-1 and HI-2 imaging higher latitude regions than during the normal phase of the mission (Harrison *et al.*, 2008). The spacecraft were separated by approximately 0.4° from Earth and were at a radial distance of 0.97 AU from the Sun.

2.2. Coronagraphic and Heliospheric Observations

On 24 January 2007 at 14:03 UT, COR-1 observed an eruption whose source region was behind the eastern limb of the Sun. At 06:43 UT on 25 January COR-1 observed a second eruption also originating from behind the Sun. The similarities between these two eruptions, as observed by LASCO coronagraphs and SECCHI/CORs, lead us to conclude that they originated from the same source region. There were two active regions (ARs) that could be the source of these eruptions, both on the back side of the Sun: AR 940, which crossed the eastern limb early on 26 January and AR 941, which crossed it around mid-day on

28 January. It is also possible that the two eruptions originated from different active regions or that they may not be associated with any active region. However, we believe that the ejections originated from AR 940, because it had a more complex topology and was the source of more activity than AR 941 as they were Earth-facing. More importantly, AR 940 was closer to the eastern limb: ARs 940 and 941 were about 24° and 43° behind the eastern limb, respectively, at the time of the first eruption. For all these reasons, we believe that AR 940 is the most likely source region for the studied limb CMEs. However, this is an assumption that may cause errors as large as 40° in the central position of the simulated ejections. Because the two STEREO spacecraft were not separated yet, it is not possible to identify the source region by triangulation as done by Howard and Tappin (2008). As they moved out of the field of view of SECCHI COR-1, these two eruptions were detected by LASCO C2 and C3 and by SECCHI COR-2.

The leading ejection was first detected in HI-1's field of view at 18:01 UT on 24 January at 4.4° elongation and was tracked until 12.1° at 04:01 UT on 25 January. At that time, there was a SECCHI data gap for 20 hours. Multiple fronts were detected in HI-2 on 26 January: The brightest one propagated from 24.7° at 02:01 UT to 32.5° at 18:01 UT. Harrison *et al.* (2008) noted the presence of "forerunner" structures (at 42° at 18:01 UT). In our previous work about these events, we focused on the observations in HI-2 on 26 January 2007 (Lugaz *et al.*, 2008). We showed that the two ejections had merged along most position angles (PAs) by the time SECCHI resumed operations. We also showed that the three brightest fronts observed in HI-2 during this day were associated with the two CMEs as well as a dense stream that had been compressed by the passage of the CMEs. The brightest front was the second one, and it was associated, depending on the PA, with the merged CMEs and with the second CME propagating into the dense sheath of the first CME.

2.3. Simulation Setup

The 3-D simulation of the two ejections was done by using the SWMF (Tóth *et al.*, 2005) as summarized in Lugaz *et al.* (2008). The entire domain is a cube of $(440\,R_\odot)^3$ centered on the Sun and divided into two subdomains: the solar corona, which is a cube of $(48\,R_\odot)^3$ centered on the Sun, and the inner heliosphere (IH), which fills the entire domain. The solar corona domain of the SWMF is resolved with 40 489 blocks of 4^3 cells each, ranging in size from $1/40\,R_\odot$ at the inner boundary to $0.75\,R_\odot$ at the outer boundary. The IH is initially resolved with 16 626 blocks of 8^3 cells each, ranging in size from $3.44\,R_\odot$ to $0.215\,R_\odot$ at its inner boundary of $16\,R_\odot$. The two domains are coupled, as explained in Tóth *et al.* (2005), via a spherical buffer that spans between $16\,R_\odot$ and $17\,R_\odot$ in the two domains. In both domains, the numerical grid at the heliospheric current sheet is refined to better capture the density gradients there. At later times, the grid in the IH is also refined during the merging of the two CMEs along the approximate location of the maximum scattering in the ecliptic plane (Thomson sphere) with cells as small as $0.215\,R_\odot$.

2.4. Solar Wind and CME Models

The solar wind and coronal magnetic field are simulated by using the model developed by Cohen *et al.* (2007). This model makes use of solar magnetogram data and the Wang – Sheeley – Arge (WSA) model (Wang, Sheeley, and Nash, 1990). In this model, the polytropic index is modified in the corona based on the value of the velocity at 1 AU from the WSA model, so that the total energy is conserved over distance along field lines (Bernoulli integral). This model has been validated in previous studies of the evolution of a CME from

the Sun to the Earth (Cohen *et al.*, 2008a, 2008b). The solar magnetic field is reconstructed from a Legendre polynomial expansion of order 49 based on NSO/SOLIS magnetogram data.[1] The initial coronal magnetic field is obtained through the potential field source surface model, before being let to relax to a nonpotential steady state, obtained by solving self-consistently the MHD equations.

To model the CMEs, we use a semicircular flux rope prescribed by a given total toroidal current, as in the model by Titov and Démoulin (1999) implemented by Roussev *et al.* (2003). This model has been used in a number of previous studies of CMEs at solar minimum (Cohen *et al.*, 2008a) and solar maximum (Tóth *et al.*, 2007), including the investigation of the merging of CMEs (Lugaz *et al.*, 2007). This flux rope solution, once superimposed on the background magnetic field, leads to immediate eruption because of force imbalance with the ambient magnetic field. The flux rope parameters are chosen such that there is an agreement with the observed values of the CME speed in the corona. The two flux ropes are initiated with the exact same parameters except for the value of the total current in the flux rope, which is 75% larger for the second ejection than for the first one. The values used for the current (3.6×10^{11} and 6.3×10^{11} A) are in good agreement with typical values derived from coronagraphic observations of CMEs (Subramanian and Vourlidas, 2009). Finally, we added the flux ropes at 14:00 UT on 24 January and 0640 UT on 25 January, in each case 3 minutes before the first observations by COR-1. The two CMEs are added onto the same position on the solar surface; therefore, they are separated by about 9° in longitude, as seen from a fixed point in the heliosphere.

Note that this model is not aimed at reproducing the complexity of the flux rope formation and the shearing motion at the surface of the Sun as in the models of Roussev, Lugaz, and Sokolov (2007), Manchester *et al.* (2008), or Lynch *et al.* (2008). Our main goals here are to study the interaction of the two ejections with the background solar wind and with each other and to compare the observations made by LASCO and SECCHI with our simulation results. Since there was no observation of the evolution of the active regions prior to or during the eruptions, a more complex model based on magnetic field observations cannot be used.

3. Evolution and Interaction of the Ejections in the Heliosphere: Filling the SECCHI Data Gap

At the launch of the second eruption, the first CME is about $55R_{\odot}$ away from the Sun with a radial speed of about 600 km s^{-1}. The speed of the first CME decreases gradually to about 450 km s^{-1} over the course of the next day until it is overtaken by the second CME. The second eruption is faster than the first one with a speed of about 1200 km s^{-1} at $20R_{\odot}$. First-order fits of the time – height profile as reported by the LASCO CME catalog for the two CMEs show that the second CME was 74% faster than the first one (1367 *versus* 785 km s^{-1}) in the upper corona. However, these speeds are for different position angles; if PA 90 is used to derive the speed for both CMEs, the difference in speed is greater (1360 *versus* 600 km s^{-1}). We, nonetheless, use a difference of 75% in the initial value of the electric current between the two CMEs as we have shown in previous studies that overtaking CMEs have less deceleration in the corona (Lugaz, Manchester, and Gombosi, 2005b) and we found this value to result in realistic velocities and deceleration in interplanetary space for the second CME.

[1] These data were obtained from the SOLIS Web site – http://solis.nso.edu.

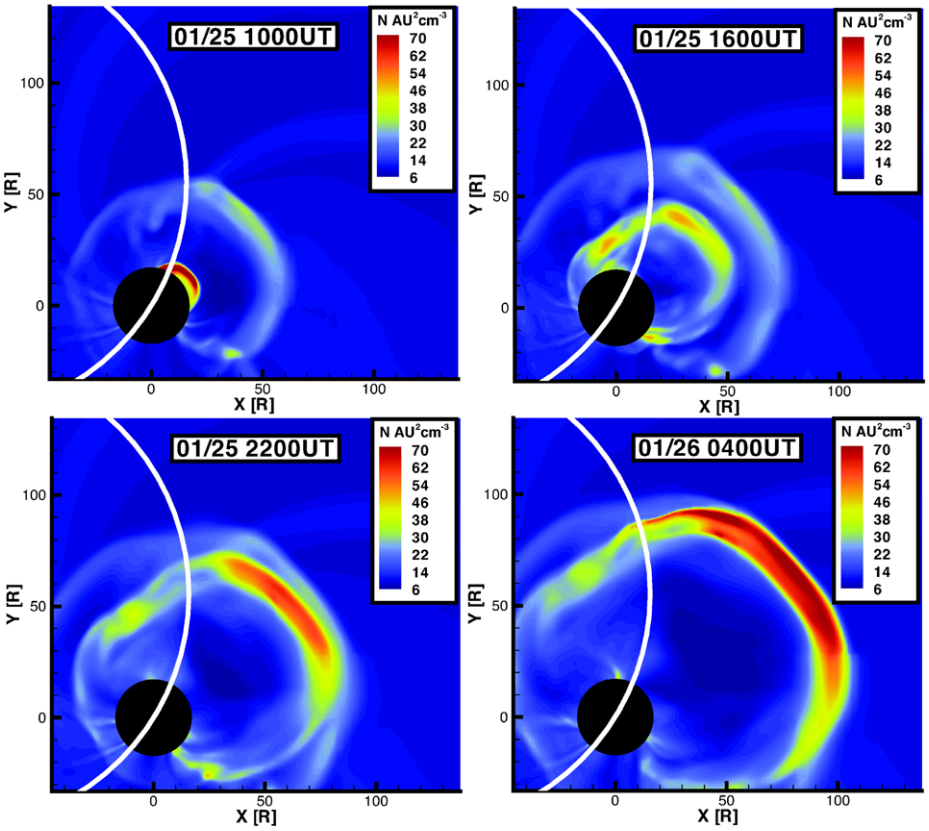

Figure 1 View of the CMEs from the solar north at four different times prior to and during their interaction showing the density scaled by $1/R^2$. The radius of the black disk is $16R_\odot$ and the white circle is the approximate projection of the Thomson sphere (relative to STEREO-A) onto the plane of the image. Earth's position is approximatively $(-179, 110, -20)R_\odot$ in this coordinate system.

Because the two eruptions are more than 16 hours apart, the second eruption propagates into a solar wind, which has essentially relaxed back to steady state (as measured in density and velocity in the open-field regions) after the passage of the preceding CME. This is different from our previous simulations of successive ejections (Lugaz, Manchester, and Gombosi, 2005b; Lugaz *et al.*, 2007) and shows that, according to our solar wind model, the solar wind relaxation time is less than 16.5 hours after an ejection. The main difference between the state of the corona before the first and second eruptions is that two streamers on both side of the erupting active regions have been deflected by the first CME and have not come back to their pre-eruption positions.

The second CME propagates into this quasi-steady solar wind (top left panel of Figure 1) until approximatively 12:00 UT on 25 January when it reaches the back of the first CME, characterized by faster speed and lower density, corresponding to the interplanetary manifestation of a magnetic cloud; the second CME front propagating into the low-density region associated with the first ejecta can be seen in the top right panel of Figure 1. There, the speed of the second CME decreases to about 1000 km s^{-1}. The second CME then reaches the back of the dense sheath associated with the first CME around 18:00 UT on 25 January and de-

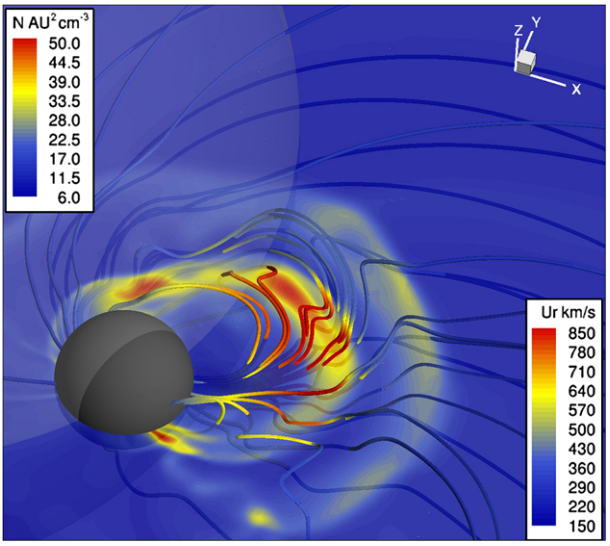

Figure 2 View of the CMEs at 16:00 UT on 25 January showing the density scaled by $1/R^2$ on the $z = 0$ plane. The black sphere radius is $17R_\odot$ and the transparent sphere is the Thomson sphere (relative to STEREO-A). The 3-D magnetic field lines are color-coded with the radial velocity.

celerates rapidly to speeds of about 800 km s^{-1}; the second CME front propagating into the first CME front can be seen in the bottom left panel of Figure 1 and also in a 3-D view at the same time on Figure 2. The two shocks have fully merged by approximatively 04:00 UT on 26 January (bottom right panel of Figure 1). The evolution of these two ejections is overall similar to what has been described in great detail in Lugaz, Manchester, and Gombosi (2005b). The speeds and positions in the description here are for the CMEs along the eastern limb (90° east of Earth); the CMEs are by nature three dimensional and this is illustrated in Figure 1, which shows the CMEs in the (solar) equatorial plane at different stages of interaction and merging, and in Figure 2, which shows a 3-D view corresponding to the top right panel of Figure 1.

According to our simulation, during the SECCHI downtime (04:00 UT to 23:59 UT on 25 January), the second ejection caught up with the first one, propagated into the lower density, faster material part of the first magnetic cloud, and reached the dense sheath of the first ejection. However, we do not expect the eruptions to have yet fully interacted for all longitudes by the time SECCHI started imaging again (00:01 UT on 26 January). This is what we reported in Lugaz *et al.* (2008), identifying two of the bright fronts observed by SECCHI/HI-2 at 02:01 UT on 26 January with the dense sheaths associated with the two CMEs.

4. Comparing Synthetic and Real Line-of-Sight Observations

4.1. Coronagraphs and Heliospheric Imagers

In Figure 3, we compare synthetic and real images of the two CMEs at three different times in the LASCO/C3 field of view. Note that, in this section, all images (synthetic or real) show total brightness. During late January 2007, there was a significant number of steady streamers (and three can be viewed in the LASCO images with their positions indicated by black arrows). The two eastern streamers were disrupted by the two CMEs; their positions after the first eruption are marked with red arrows. We are able to capture the disruption of

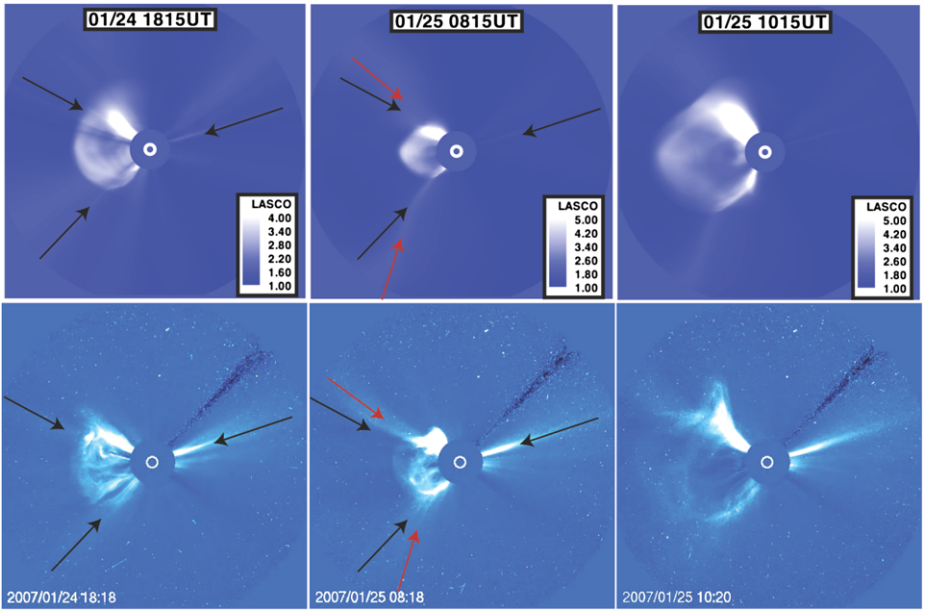

Figure 3 Comparison of synthetic (top) and real (bottom) LASCO/C3 images at three different time instants, showing total brightness (divided by the monthly background for the synthetic images). The positions of streamers before the first ejection are shown approximatively with black arrows (same direction for synthetic and simulated images); the deflected streamers positions are indicated with the red arrows.

these streamers with our synthetic images by calculating a synthetic "monthly" background in a way similar to the procedure done for real line-of-sight images. From our steady state, we produce 27 synthetic images by positioning satellites separated by increments of 13° in the ecliptic plane, to simulate the effects of a full solar rotation, with each image representing the LASCO approximate view on a different day of the Carrington rotation; the background image is calculated from this by taking, for each pixel, the minimum value of the 27 images. Comparing the first and third columns of Figure 3, one can see that the streamer around PA 120 is still significantly deflected in front of the second CME as compared to its pre-eruption value. The "flattening" and associated "dimple" of the second CME front around PA 40, which can be seen in the real and synthetic images, is due to the second CME propagating into one of these deflected streamers.

In Figure 4, we compare synthetic images of the two CMEs in the heliosphere from the point of view of STEREO-A with real images when available. There is also an online animation combining the synthetic line-of-sight images from LASCO and the HIs into one continuous movie covering over 3 days. There is a fair agreement between the overall shape and position of the CME in real and synthetic images of the first CME (left column of Figure 4). However, the CME in the synthetic image extends significantly north of the bright feature corresponding to the northeast streamer. This might be due to an overexpansion of the flux rope CME owing to the unrealistic CME initiation mechanism. The CME also appears significantly brighter in the synthetic image compared to the real one. This might be partly explained by the difference in the background-subtraction mechanism. Next, we show an example of an HI-1 image during SECCHI downtime corresponding to the top left image in Figure 1 and Figure 2 (*i.e.*, at the start of the interaction between the CMEs). This demonstrates that HI-1 would have been able to clearly observe the two CME fronts at the

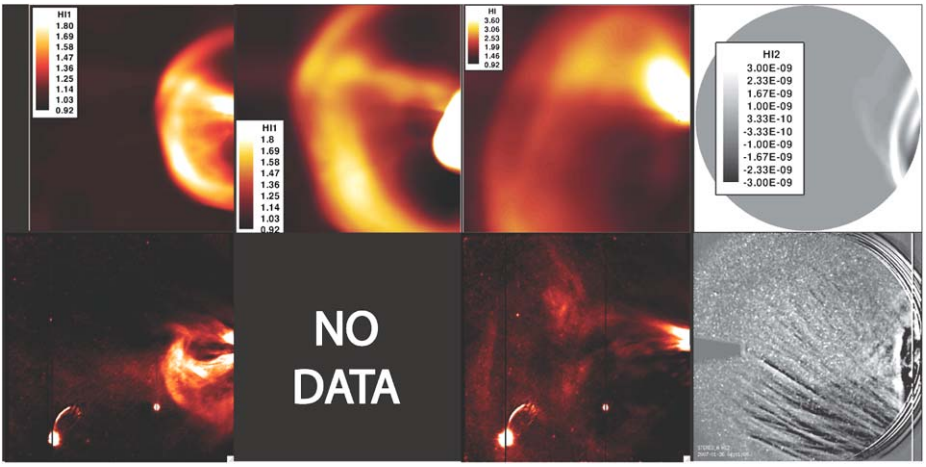

Figure 4 Comparison of synthetic (top) and real (bottom) SECCHI/HI images. The first three columns are HI-1-A images (background-divided for the synthetic images), the last one HI-2 images (2-hour running difference). The times, from left to right, are 02:00 UT and 10:00 UT on 25 January and 00:00 UT and 04:00 UT on 26 January. There were no SECCHI observations between 06:00 UT and 23:00 UT on 25 January. The real HI-1 images are processed by the NRGF.

same time, allowing for a more direct comparison of the CME evolution in the heliosphere. We believe that the image at 00:01 UT on 26 January, once processed by the Normalized Radial Graded Filter (NRGF; see Morgan, Habbal, and Woo, 2006) shows evidence of the second CME front exiting the instrument field of view. This is confirmed by an analysis of a time sequence of our synthetic images that show the second front propagating inside the first one starting at 18:00 UT on January 25 (see animation appended to the electronic version). Last, we show one example of an HI-2 image at the same time as the bottom right image in Figure 1. One has to remember that the plane in Figure 1 corresponds to PA 90, which is rolled counterclockwise by approximately 21.7° in the images in Figure 4. As analyzed in Lugaz *et al.* (2008), the brightest front corresponds to the merged CMEs whereas the very dim leading front corresponds to part of the first front along PAs close to the Thomson sphere (TS) that have not yet been overtaken by the second CME.

4.2. Time-Elongation Maps

Since qualitative comparisons between synthetic and real white-light observations show that the simulation offers an accurate enough reproduction of the observations, it is now important to compare more quantitatively simulated and real images. One of the methods to study the evolution of density enhancements is to produce time-elongation maps (J-maps) for different PAs (Sheeley *et al.*, 1997, 2008; Rouillard *et al.*, 2008; Davies *et al.*, 2009). Such maps allow for the tracking of CMEs to large elongation angles and the study of their evolution without assumptions concerning the direction of propagation. In this section, we discuss J-maps along two PAs – 90 and 69 – corresponding to the approximate "nose" of the CMEs and the apparent central angle of the SECCHI instruments, respectively. Synthetic and real maps are shown in Figure 5; we first identify the tracks seen in these maps before comparing them quantitatively.

For the synthetic J-map, we take a slice every 20 minutes and plot the difference of the total brightness with the slice 2 hours earlier. For the real J-map, a slice is taken for every

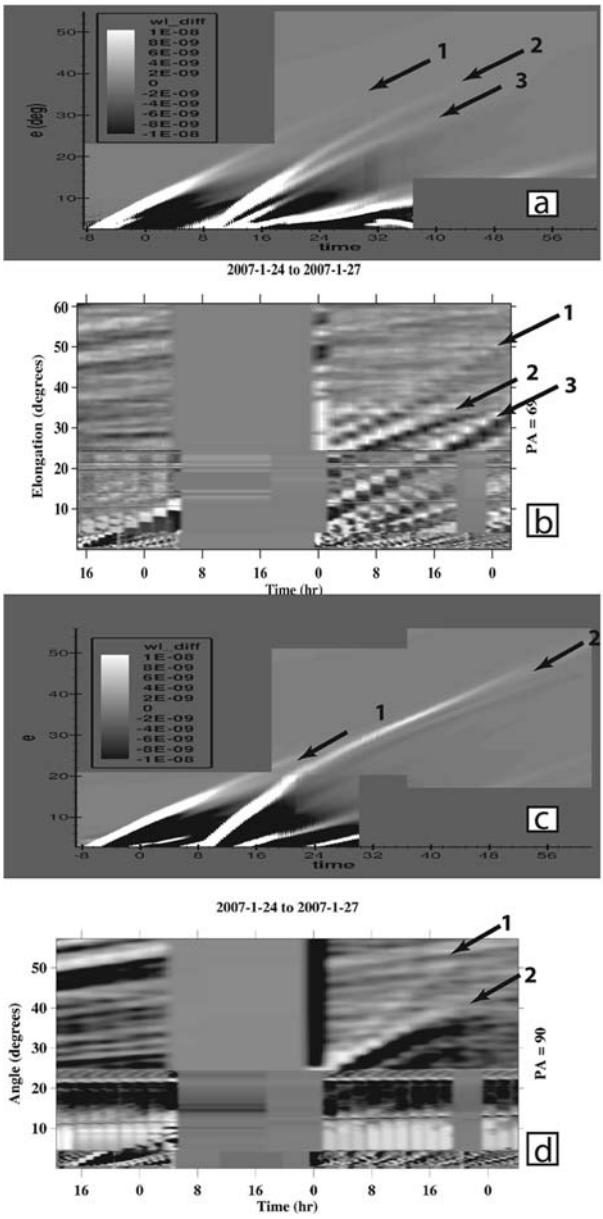

Figure 5 Comparison of synthetic (a and c) and real (b and d) J-maps for PA 69 (a and b) and PA 90 (c and d). PA 69 is the center of the HI images whereas PA 90 is closer to the "nose" of the CMEs. Time starts at 16:00 UT on 24 January (corresponding to −8 on panels a and c and the first 16 on panels b and d).

observation (*i.e.*, every 2 hours for HI-2 and varying between every 20 minutes and every hour for HI-1) and the running difference is plotted. The higher cadence makes the synthetic J-maps look "smoother," but because we take a 2-hour running difference, the width and slope of the tracks have the same meaning as for the real maps. SECCHI instruments did not image from 04:00 UT on 25 January to 00:00 UT on 26 January. The presence of Venus makes the HI-1 data near PA 90 difficult to use.

In the synthetic J-map at PA 69, there are three main distinct tracks (marked with black arrows). They correspond to the three fronts described in Lugaz *et al.* (2008): the first ejection, the second ejection, and a dense stream (tracks 1 to 3, respectively). The dense stream is first compressed by the first CME and can be seen around 08:00 UT on 25 January behind the first CME. The compressed (respectively, uncompressed) stream can be seen ahead of (respectively, behind) the first CME in the top left panel of Figure 1. At 04:00 UT on 26 January, there are three fronts past 20° elongation (*i.e.*, in the HI-2 field of view), the brightest one corresponding to the second CME. Noteworthy is the fact that the two CMEs do not appear to merge along this PA and that the track of the first CME becomes very faint past 30° elongation.

The real J-map at this PA is much more complicated and harder to analyze in part owing to the lack of observations on 25 January. There also appears to be three main tracks visible in HI-2 starting at about 14:00 UT on 26 January. We believe that these three tracks correspond to the fronts identified in the synthetic image in the same order. One apparent problem with this interpretation is that track 1 has the fastest angular speed of all and can be tracked the farthest until about 60° elongation, whereas track 2 (corresponding to the second eruption, in this interpretation) is the brightest but fades away quickly past 35° elongation. According to our analysis, track 1 initially (in HI-1) corresponds to the first CME and at later times (in HI-2) to the merged CMEs, which explains the faster angular speed there. This track corresponds to the "forerunner" structures described by Harrison *et al.* (2008). Making a definitive identification regarding the origin of track 1 would require knowing whether tracks 1 and 2 merge during SECCHI downtime, since the explanation just described would require the two tracks to merge when the two CME fronts collide. If this analysis is correct, there is one important aspect that the simulation does not capture: the fading of the second (and brightest) front. The most likely explanation is that this front and its brightening are associated with a temporary phenomenon: the propagation of the second CME inside the first dense sheath, resulting in a twice compressed medium. As the CMEs merge, front 2 corresponds to the density peak of the twice-compressed sheath, whereas front 1 corresponds to the new sheath associated with the merged CMEs, similar to what is explained in Lugaz, Manchester, and Gombosi (2005b). However, the second density peak eventually relaxes, resulting in the rapid fading of track 2. This phenomenon does not happen in the synthetic line-of-sight images, but it would happen if the merging happened approximatively at the same time along all directions. In our simulation, as described in the next section and as seen in Figure 1, the two CMEs do not merge until 02:00 UT on 27 January along the TS.

In the synthetic J-map at PA 90, there are only two main distinct tracks, corresponding to the two ejections. The dense stream (which corresponds to track 3 at PA 69) does not appear at this PA, reflecting the 3-D nature of the heliosphere and giving us an additional clue that this feature is not due to a CME (as explained in Lugaz *et al.*, 2008). Along this angle, there is complete merging of the fronts around 06:00 UT on 26 January. The merging is associated with a brightening of the front, especially noticeable between 08:00 UT and 18:00 UT on 26 January. The real J-map also shows only two tracks with the second one brighter, but they appear to diverge from a similar (merged) position at the start of the observations on 26 January. Similarly to the J-map at PA 69, we believe track 2 is associated with the merging of the ejections (propagation of the second front inside the first one) whereas track 1 is associated with the first ejection and later on with the merged ejections. In our synthetic images, there is also a splitting of the merged front along PA 90 starting around 02:00 UT on 27 January, as can be seen in the online animation. This corresponds more or less to the time of the merging of the CME fronts along the TS in the simulation.

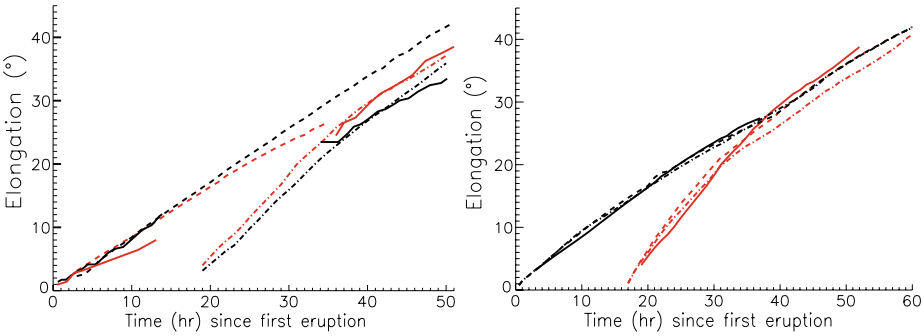

Figure 6 Time-elongation profiles from the observations, synthetic images, and profiles derived from the 3-D simulation. The left panel shows a comparison of the real (solid) and synthetic (dashed: first eruption; dash-dotted: second eruption) elongation angles for PA 69 (red) and PA 90 (black). The right panel shows a comparison of the synthetic elongation (solid) and elongation from the simulation on the limb (dashed) and on the Thomson sphere (dash-dotted) for PA 90 for the first (black) and second (red) eruptions.

4.3. Time-Elongation and Time – Height Plots

Next, we focus on the quantitative comparison between observed and synthetic positions from the J-maps, focusing on the two CMEs (tracks 1 and 2 according to the analysis just presented). The left panel of Figure 6 confirms without doubt that the brighter front observed in HI-2 corresponds to the second eruption (PA 69) or the merged eruptions (PA 90). The model is in good agreement with observations except at large elongation angles (past 30°), starting approximatively 45 hours after the first eruption. This might be due, for example, to the complexity of tracking dim fronts in the real images, or to some observational effects not being well reproduced by the synthetic line-of-sight procedure. We can now compare the position derived from the line-of-sight images with that from our 3-D simulation to determine which parts of the CME are being tracked.

In the right panel of Figure 6, we show this comparison for PA 90 (the "nose" of the ejections). The solid, dashed, and dash-dotted lines show the elongation angles of the CME fronts in the synthetic line of sight, 90° from STEREO-A, and on the TS, respectively. The TS is the locus of maximum scattering (Jackson and Leinert, 1985; Vourlidas and Howard, 2006). It comes from the fact that the scattering along a given line of sight is maximized at the point of closest approach to the Sun. Since the source region of the CMEs was behind the eastern limb of the Sun, assuming that the CMEs are propagating along the limb (90° from STEREO) is the best approximation that can be made. By analyzing this figure, we can see that, for the first eruption, the line-of-sight position is always within 1° of the real one. The position can, then, be estimated with minimal error by $R_{\rm CME} = d_{\rm STEREO} \tan(\epsilon)$, where $d_{\rm STEREO} = 0.97$ AU is the heliospheric distance of STEREO-A, ϵ is the elongation angle, and $R_{\rm CME}$ is the position of the CME 90° away from STEREO-A. From this position, the speed and heliospheric deceleration of the first CME can then be relatively well constrained up to about $90 R_{\odot}$.

For the second CME, we must distinguish the periods before and after the CME – CME interaction. Before the interaction (until about 30 hours), assuming that the observed position corresponds to the position on the TS is a better approximation than the "limb" approximation. For example, at time $t = 28$ hours, the position on the TS is 16.2°, on the limb (90° from STEREO-A) it is 17.5°, and from the synthetic line of sight it is 15.5° (as seen in the right panel of Figure 6).

At large elongation angles, one must also consider the curvature of the CMEs and the effect of the TS to determine the radial distances. Assuming a propagation along the limb (or any fixed angular position) may result in a large overestimation of the position. For example, at time $t = 52$ hours (18:00 UT on 26 January), the dim front along PA 69 is at 43.3°, which is similar to the "forerunner" front at 42° described by Harrison *et al.* (2008). This angular position corresponds to radial positions of $145R_{\odot}$, if one assumes that the emission originates from the TS, yet $200R_{\odot}$, if one assumes it originates from the limb (90° E). In fact, based on our simulation, the front of the first CME was at about $145R_{\odot}$ on the TS but only $160R_{\odot}$ at 90°.

However, knowing the deprojected distances along the TS does not allow for the determination of the true CME speed. This is because, at each time instant, the position on the TS corresponds to a different part of the CME and a time – height profile derived from these positions is not consistent with tracking the same part of the CME along a fixed direction. Therefore such a profile would show an apparent acceleration or deceleration of the CME based on its interaction with the TS. In contrast to LASCO observations where the bright fronts were tracked for hours, tracking density enhancements for days with SECCHI does not allow us to use a simple approximation such as the "plane-of-sky" one. Therefore, the best way to use the information provided by the line-of-sight images is to assume that the CME is spherically symmetric. Then, the position on the TS can be assumed to correspond to the position along any direction. For the example given here, this is a better approximation than assuming the bright front is at 90° ($15R_{\odot}$ underestimation versus $40R_{\odot}$ overestimation of the actual position). Other spurious effects, such as the appearance of multiple bright fronts in the line-of-sight images associated with one CME front, are expected to appear at very large elongation angles (Manchester *et al.*, 2008).

5. Discussion and Conclusion

We have investigated the heliospheric evolution and interaction of the two coronal mass ejections during 24 – 27 January 2007 using a numerical MHD simulation to interpret and better analyze observations by the SECCHI suite aboard STEREO. We are able to reproduce successfully the observations in the LASCO field of view. Using a realistic background-subtraction procedure for the synthetic line-of-sight images, we are able to reproduce observations of streamer deflections and to relate the position of the new streamer with a deformation and "flattening" of the second CME along some position angles.

We have proven that STEREO has the ability to make indisputable observations of a CME catching up with a previous one, which would help constrain numerical models of CME – CME interaction. By assuming no deceleration of the two CMEs and using the time – height data from LASCO, the merging of the two CMEs was expected to happen around 21:00 UT on 25 January around 25° elongation. We, in fact, find evidence that the CMEs had just merged at the beginning of 26 January when SECCHI started observing again. In our simulation, the merging happens around 06:00 UT on 26 January. We believe that the bright front around elongation 20° – 24° in the HI-1 image at 00:00 UT and 02:00 UT on 26 January corresponds to the front of the second CME propagating inside the front of the first CME or a second density peak associated with twice-shocked medium. There were also observations by SMEI of one bright front from the end of 25 January to about 08:00 UT on 26 January whose position corresponds with that of the second front (brightest) in our J-maps (D. Webb, private communication). We believe another front, which can be seen in the SMEI images from 12:00 UT on 27 January to 06:00 UT on 28 January, mostly at large PAs (up to 120°),

corresponds to front 1 in the J-maps. Merging of the SMEI and SECCHI data will probably help tracking density structures in the heliosphere, but careful cross-calibration of the two instruments is required first.

Finally, our simulation helps us identify the different tracks in time-elongation maps (J-maps) of the CMEs and relate the elongation angles to the actual positions of the CME fronts. We find tracks associated with the two CME fronts, the merged front, and a dense stream. The time-elongation profile of the brightest front associated with the CMEs is in good agreement qualitatively and quantitatively with J-maps constructed from observations. However, there is one important aspect where our model differs from observations: In the real images, the brightest front, which corresponds initially to the second CME, rapidly fades after the CME – CME merging, whereas in our synthetic images, the initially dimmest front, corresponding to the first CME, is the one that fades quickly. One possible explanation is that the second front after the CME – CME merging, in the real images, is associated with the presence of a second density peak in the merged sheath associated with the twice-compressed medium (as discussed in Lugaz, Manchester, and Gombosi, 2005b). Our simulation may not capture this in the line-of-sight images for a number of reasons, including limited spatial resolution, asymmetry of the second eruption, and late merging of the CME fronts.

Rouillard *et al.* (2008) associated a bright front observed in J-maps with *in situ* observations of a corotating interaction region at L1. Here, it is not possible to make such an association, because the CMEs did not hit Earth. However, the simulation allows us to fill the SECCHI data gap and to explain the difference in the number of tracks in different PAs. We found that one of the observed fronts can be tracked until about 60°, which corresponds to 0.85 AU on the Thomson sphere and about 1.75 AU if one assumes a point source propagating 90° away from Earth. The latter position is not consistent with the CME speed and time evolution (barring dramatic late acceleration). Therefore, it proves that HI-2 (and SMEI at large elongation angles) essentially captures the propagation of the CMEs onto the Thomson sphere surface. This behavior was predicted by Vourlidas and Howard (2006). This fact should complicate the direct use of HI data to derive a true speed for the CMEs or to test heliospheric drag models. The procedure followed here is to use a numerical simulation with synthetic imaging capabilities to derive the likely speed, deceleration, and interaction of the CMEs. The first step is to make sure the synthetic observations reproduce successfully the real observations, before determining the CME position in three dimensions. We also show that, in the absence of 3-D numerical models and triangulation of the CMEs by the two STEREO spacecraft, assuming spherical symmetry of the CME and deriving its position from the projection on the Thomson sphere is the most accurate way to determine the best approximation of the "true" position of the CME front. It is also possible that a number of case studies of events observed by SECCHI/HIs will help to develop a paradigm to obtain time – height profiles from heliospheric imagers, using for example 3-D reconstructions of the CMEs such as done by Howard and Tappin (2008).

Acknowledgements The research for this manuscript was supported by NSF Grant Nos. ATM-0639335 and ATM-0819653 as well as NASA Grant Nos. NNX-07AC13G and NNX-08AQ16G. N.L. would also like to acknowledge travel support from SPS to participate at the European Solar Physics Meeting in Freiburg to present these results and to thank D. Webb and V. Bothmer for discussion about these eruptions at the IAU 257 Symposium and EGU meeting, respectively. The simulation reported here was carried out on a dedicated cluster of the solar group at the Institute for Astronomy. We would like to thank the reviewer for helping us to improve and to clarify this manuscript. SOLIS data were obtained from the NSO Web site. The SECCHI data are produced by an international consortium of the Naval Research Laboratory, Lockheed Martin Solar and Astrophysics Laboratory and NASA Goddard Space Flight Center (USA), Rutherford Appleton Laboratory and University of Birmingham (UK), Max-Planck-Institut für Sonnensystemforschung (Germany), Centre

Spatiale de Liege (Belgium), and Institut d'Optique Théorique et Appliquée and Institut d'Astrophysique Spatiale (France). SOHO is a project of international cooperation between ESA and NASA, and the SOHO LASCO/EIT catalogs are maintained by NASA, the Catholic University of America, and the US Naval Research Laboratory (NRL).

References

Berdichevsky, D., Bougeret, J.L., Delaboudinière, J.P., Fox, N., Kaiser, M., Lepping, R., Michels, D., Plunkett, S., Reames, D., Reiner, M., Richardson, I., Rostoker, G., Steinberg, J., Thompson, B., von Rosenvinge, T.: 1998, *Geophys. Res. Lett.* **25**, 2473. doi:10.1029/97GL03771.

Brueckner, G.E., Howard, R.A., Koomen, M.J., Korendyke, C.M., Michels, D.J., Moses, J.D., Socker, D.G., Dere, K.P., Lamy, P.L., Llebaria, A., Bout, M.V., Schwenn, R., Simnett, G.M., Bedford, D.K., Eyles, C.J.: 1995, *Solar Phys.* **162**, 357. doi:10.1007/BF00733434.

Chané, E., van der Holst, B., Jacobs, C., Poedts, S., Kimpe, D.: 2006, *Astron. Astrophys.* **447**, 727. doi:10.1051/0004-6361:20053802.

Chen, J., Krall, J.: 2003, *J. Geophys. Res.* **108**, 1410. doi:10.1029/2003JA009849.

Cohen, O., Sokolov, I.V., Roussev, I.I., Arge, C.N., Manchester, W.B., Gombosi, T.I., Frazin, R.A., Park, H., Butala, M.D., Kamalabadi, F., Velli, M.: 2007, *Astrophys. J.* **654**, L163. doi:10.1086/511154.

Cohen, O., Sokolov, I.V., Roussev, I.I., Lugaz, N., Manchester, W.B.I., Gombosi, T.I., Arge, C.N.: 2008a, *J. Atmos. Solar-Terr. Phys.* **70**, 583. doi:10.1016/j.jastp.2007.08.065.

Cohen, O., Sokolov, I.V., Roussev, I.I., Gombosi, T.I.: 2008b, *J. Geophys. Res.* **113**, 03104. doi:10.1029/2007JA012797.

Davies, J.A., Harrison, R.A., Rouillard, A.P., Sheeley, N.R., Perry, C.H., Bewsher, D., Davis, C.J., Eyles, C.J., Crothers, S.R., Brown, D.S.: 2009, *Geophys. Res. Lett.* **36**, 02102. doi:10.1029/2008GL036182.

Gopalswamy, N., Yashiro, S., Michałek, G., Kaiser, M.L., Howard, R.A., Reames, D.V., Leske, R., von Rosenvinge, T.: 2002, *Astrophys. J.* **572**, L103.

Harrison, R.A., Davis, C.J., Eyles, C.J., Bewsher, D., Crothers, S.R., Davies, J.A., Howard, R.A., Moses, D.J., Socker, D.G., Newmark, J.S., Halain, J.P., Defise, J.M., Mazy, E., Rochus, P., Webb, D.F., Simnett, G.M.: 2008, *Solar Phys.* **247**, 171. doi:10.1007/s11207-007-9083-6.

Howard, R.A., Moses, J.D., Vourlidas, A., Newmark, J.S., Socker, D.G., Plunkett, S.P., Korendyke, C.M., Cook, J.W., Hurley, A., Davila, J.M., Thompson, W.T., St Cyr, O.C., Mentzell, E., Mehalick, K., Lemen, J.R., Wuelser, J.P., Duncan, D.W., Tarbell, T.D., Wolfson, C.J., Moore, A., Harrison, R.A., Waltham, N.R., Lang, J., Davis, C.J., Eyles, C.J., Mapson-Menard, H., Simnett, G.M., Halain, J.P., Defise, J.M., Mazy, E., Rochus, P., Mercier, R., Ravet, M.F., Delmotte, F., Auchere, F., Delaboudinière, J.P., Bothmer, V., Deutsch, W., Wang, D., Rich, N., Cooper, S., Stephens, V., Maahs, G., Baugh, R., McMullin, D., Carter, T.: 2008, *Space Sci. Rev.* **136**, 67. doi:10.1007/s11214-008-9341-4.

Howard, T.A., Tappin, S.J.: 2008, *Solar Phys.* **252**, 373. doi:10.1007/s11207-008-9262-0.

Jackson, B.V., Leinert, C.: 1985, *J. Geophys. Res.* **90**, 10759. doi:10.1029/JA090iA11p10759.

Lugaz, N., Manchester, W.B., Gombosi, T.I.: 2005a, *Astrophys. J.* **627**, 1019.

Lugaz, N., Manchester, W.B., Gombosi, T.I.: 2005b, *Astrophys. J.* **634**, 651.

Lugaz, N., Manchester, W.B., Roussev, I.I., Tóth, G., Gombosi, T.I.: 2007, *Astrophys. J.* **659**, 788. doi:10.1086/512005.

Lugaz, N., Vourlidas, A., Roussev, I.I., Jacobs, C., Manchester, W.B. IV, Cohen, O.: 2008, *Astrophys. J.* **684**, L111. doi:10.1086/592217.

Lynch, B.J., Antiochos, S.K., DeVore, C.R., Luhmann, J.G., Zurbuchen, T.H.: 2008, *Astrophys. J.* **683**, 1192. doi:10.1086/589738.

Manchester, W.B., Gombosi, T.I., Roussev, I., De Zeeuw, D.L., Sokolov, I.V., Powell, K.G., Tóth, G., Opher, M.: 2004, *J. Geophys. Res.* **109**, 1102. doi:10.1029/2002JA009672.

Manchester, W.B., Vourlidas, A., Tóth, G., Lugaz, N., Roussev, I.I., Sokolov, I.V., Gombosi, T.I., De Zeeuw, D.L., Opher, M.: 2008, *Astrophys. J.* **684**, 1448. doi:10.1086/590231.

Morgan, H., Habbal, S.R., Woo, R.: 2006, *Solar Phys.* **236**, 263. doi:10.1007/s11207-006-0113-6.

Odstrcil, D., Riley, P., Zhao, X.P.: 2004, *J. Geophys. Res.* **109**, A02116. doi:10.1029/2003JA010135.

Odstrcil, D., Pizzo, V.J., Arge, C.N.: 2005, *J. Geophys. Res.* **110**, A02106. doi:10.1029/2004JA010745.

Odstrcil, D., Vandas, M., Pizzo, V.J., MacNeice, P.: 2003, In: Velli, M., Bruno, R., Malara, F., Bucci, B. (eds.) *Tenth International Solar Wind Conf., AIP Conf. Proc.* **679**, 699. doi:10.1063/1.1618690.

Odstrčil, D., Pizzo, V.J.: 1999, *J. Geophys. Res.* **104**, 483. doi:10.1029/1998JA900019.

Riley, P., Lionello, R., Mikić, Z., Linker, J.: 2008, *Astrophys. J.* **672**, 1221. doi:10.1086/523893.

Rouillard, A.P., Davies, J.A., Forsyth, R.J., Rees, A., Davis, C.J., Harrison, R.A., Lockwood, M., Bewsher, D., Crothers, S.R., Eyles, C.J., Hapgood, M., Perry, C.H.: 2008, *Geophys. Res. Lett.* **35**, L10110. doi:10.1029/2008GL033767.

Roussev, I.I., Sokolov, I.V.: 2006, In: Gopalswamy, N., Mewaldt, R., Torsti, J. (eds.) *Models of Solar Eruptions: Recent Advances From Theory and Simulations, in Solar Eruptions and Energetic Particles*, *Geophys. Monograph Ser.* **165**, AGU, Washington, 89. doi:10.1029/165GM10.

Roussev, I.I., Lugaz, N., Sokolov, I.V.: 2007, *Astrophys. J.* **668**, L87. doi:10.1086/522588.

Roussev, I.I., Gombosi, T.I., Sokolov, I.V., Velli, M., Manchester, W., DeZeeuw, D.L., Liewer, P., Tóth, G., Luhmann, J.: 2003, *Astrophys. J.* **595**, L57.

Schwenn, R., Raymond, J.C., Alexander, D., Ciaravella, A., Gopalswamy, N., Howard, R., Hudson, H., Kaufmann, P., Klassen, A., Maia, D., Munoz-Martinez, G., Pick, M., Reiner, M., Srivastava, N., Tripathi, D., Vourlidas, A., Wang, Y.M., Zhang, J.: 2006, *Space Sci. Rev.* **123**, 127. doi:10.1007/s11214-006-9016-y.

Sheeley, N.R. Jr., Wang, Y.M., Hawley, S.H., Brueckner, G.E., Dere, K.P., Howard, R.A., Koomen, M.J., Korendyke, C.M., Michels, D.J., Paswaters, S.E., Socker, D.G., St Cyr, O.C., Wang, D., Lamy, P.L., Llebaria, A., Schwenn, R., Simnett, G.M., Plunkett, S., Biesecker, D.A.: 1997, *Astrophys. J.* **484**, 472. doi:10.1086/304338.

Sheeley, N.R. Jr., Herbst, A.D., Palatchi, C.A., Wang, Y.M., Howard, R.A., Moses, J.D., Vourlidas, A., Newmark, J.S., Socker, D.G., Plunkett, S.P., Korendyke, C.M., Burlaga, L.F., Davila, J.M., Thompson, W.T., St Cyr, O.C., Harrison, R.A., Davis, C.J., Eyles, C.J., Halain, J.P., Wang, D., Rich, N.B., Battams, K., Esfandiari, E., Stenborg, G.: 2008, *Astrophys. J.* **674**, L109. doi:10.1086/529020.

Subramanian, P., Vourlidas, A.: 2009, *Astrophys. J.* **693**, 1219. doi:10.1088/0004-637X/693/2/1219.

Sun, W., Deehr, C.S., Dryer, M., Fry, C.D., Smith, Z.K., Akasofu, S.I.: 2008, *Space Weather* **6**, S03006. doi:10.1029/2006SW000298.

Titov, V.S., Démoulin, P.: 1999, *Astron. Astrophys.* **351**, 707.

Titov, V.S., Mikic, Z., Linker, J.A., Lionello, R.: 2008, *Astrophys. J.* **675**, 1614. doi:10.1086/527280.

Tóth, G., Sokolov, I.V., Gombosi, T.I., Chesney, D.R., Clauer, C.R., De Zeeuw, D.L., Hansen, K.C., Kane, K.J., Manchester, W.B., Oehmke, R.C., Powell, K.G., Ridley, A.J., Roussev, I.I., Stout, Q.F., Volberg, O., Wolf, R.A., Sazykin, S., Chan, A., Yu, B., Kóta, J.: 2005, *J. Geophys. Res.* **110**, A12226. doi:10.1029/2005JA011126.

Tóth, G., De Zeeuw, D.L., Gombosi, T.I., Manchester, W.B., Ridley, A.J., Roussev, I.I., Sokolov, I.V.: 2007, *Space Weather* **5**, S06003. doi:10.1029/2006SW000272.

Vourlidas, A., Howard, R.A.: 2006, *Astrophys. J.* **642**, 1216. doi:10.1086/501122.

Wang, Y.M., Sheeley, N.R. Jr., Nash, A.G.: 1990, *Nature* **347**, 439. doi:10.1038/347439a0.

Webb, D.F., Howard, T.A., Fry, C.D., Odstricil, D.: 2008, *AGU Spring Meeting Abstracts*, 21.

Wu, C.C., Fry, C.D., Wu, S.T., Dryer, M., Liou, K.: 2007, *J. Geophys. Res.* **112**, A09104. doi:10.1029/2006JA012211.

Xiong, M., Zheng, H., Wang, Y., Wang, S.: 2006, *J. Geophys. Res.* **111**, A08105. doi:10.1029/2005JA011593.

Zhang, J., Richardson, I.G., Webb, D.F., Gopalswamy, N., Huttunen, E., Kasper, J.C., Nitta, N.V., Poomvises, W., Thompson, B.J., Wu, C.C., Yashiro, S., Zhukov, A.N.: 2007, *J. Geophys. Res.* **112**, A10102. doi:10.1029/2007JA012321.